Asociación Argentina
de Mecánica Computacional

Mecánica Computacional Vol XXIX, págs. 7711-7723 (artículo completo)
Eduardo Dvorkin, Marcela Goldschmit, Mario Storti (Eds.)
Buenos Aires, Argentina, 15-18 Noviembre 2010

NUMERICAL SIMULATIONS OF DUCTILE CRACK GROWTH ON CIRCUMFERENTIALLY FLAWED PIPES UNDER COMBINED LOAD CONDITIONS

Sebastian Cravero, Richard E. Bravo and Hugo A. Ernst

Tenaris, Investigación y desarrollo, Dr. J. A. Simin 250, 2804 Campana, Argentina

Keywords: Computational Fracture Mechanics, J-integral, Crack-tip Constraint, Gurson Model.

Abstract. For certain applications, pipelines may be submitted to biaxial loading situations. In these cases, it is not clear the influence of the biaxiality on the fracture mechanics behavior of cracked pipelines. For further understanding of biaxial loading effects, this work presents a numerical simulation of ductile tearing in a circumferentially surface cracked pipe under combined loading conditions using the computational cell methodology. The model was adjusted with experimental results obtained in laboratory using single edge cracked under tension (SENT) specimens. These specimens appear as a better alternative to conventional fracture specimens to characterize fracture toughness of circumferentially cracked pipes. The negligible effect of biaxial loadings on resistance curves was demonstrated.

To guarantee the similarities of stress and strains fields between SENT specimens and cracked pipes subjected to internal pressure plus bending, a constraint study using the *J-Q* methodology and the *h* parameter was used. The constraint study gives information about the characteristics of the crack-tip conditions.

1 INTRODUCTION

Onshore and offshore pipelines can be submitted to loadings beyond yielding during installation and in-service conditions. Particular conditions, as heating and cooling cycles, ground movement and frost heave, may produce yielding in the pipe metal. These situations may cause that cracks, formed during fabrication or in service, being loaded under biaxial conditions. Current fracture assessment procedures were mainly developed for uniaxial loading conditions. However, biaxial loading situations may have an effect on the pipe material toughness (J resistance curve) and the crack driving force (i.e.: CTOD (Wells, 1961), J-integral (Rice, 1968)). Hence, it seems to be necessary the development of fracture assessment methodologies considering combined loading conditions (i.e.: Bending + Int. Pressure, Tension + Bending + Int. Pressure) that produce biaxiality.

To further understand biaxiality effects on fracture mechanics of cracked pipelines, this work presents a numerical simulation of ductile tearing in a circumferentially surface cracked pipe under biaxial loading using the computational cell methodology to study the biaxial loading effects on tearing behavior. The model was adjusted with experimental results obtained in laboratory using single edge cracked under tension (SENT) specimens.

To assess the similarities of stress and strains fields between SENT specimens and cracked pipes subjected to biaxial loading, a constraint study using the J-Q methodology was applied. The objective is to examine combined loading effects on the correlation of fracture behavior for the analyzed cracked configurations using the Q (O'Dowd and Shih, 1991) and h (Brocks and Schmitt, 1993) parameters.

The Q parameter measures the deviation of the stress field of the studied geometry from a reference stress solution (i.e. the boundary layer model (Rice, 1967)). On the other hand, the h parameter is defined as the ratio of the hydrostatic stress level ahead of the crack front over the effective Von Mises stress and it characterizes the growth of micro voids in a triaxial stress field.

2 DUCTILE TEARING NUMERICAL SIMULATION

2.1 Constitutive Model

The numerical computations for the fracture specimens and cracked pipes analyzed in this work are generated using the research code WARP3D (Koppenhoefer, et. al, 1994). The analyses utilize an elastic-plastic constitutive model with J_2 flow theory and conventional Mises plasticity using large strain theory. The numerical solutions employ a simple piecewise stress-strain curve where the yield stress is 479 MPa and the elasticity modulus is, E = 206 GPa and ν = 0.3. Figure 1 compares the true stress strain curve experimentally obtained with the input for the model.

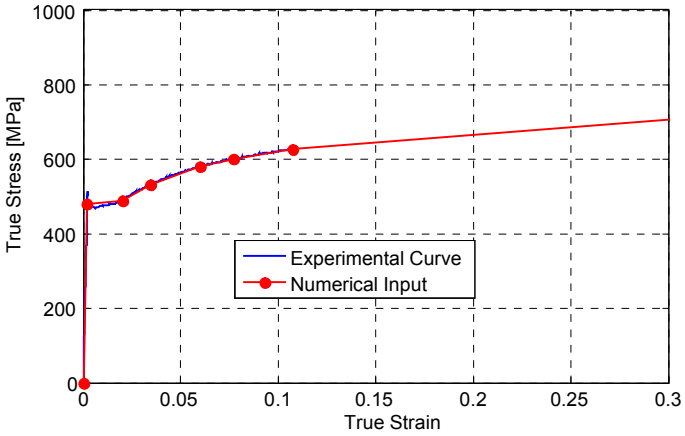

Figure. 1: True stress-strain curve

A model was constructed to simulate stable crack growth and to study the effect of biaxial loading on the resistance curves. The simulation is based on the computational cell methodology (Xia and Shih, 1995). This methodology is used to predict ductile resistance curves of cracked specimens. The fracture is assumed to propagate in the plane containing the defect which is formed by computational cells with dimension D defining the thickness of the layer were the damage occurs. The cells have initial void volume fraction denoted by f_0, with no subsequent void nucleation. Progressive void growth and macroscopic material softening in each cell are described with the Gurson-Tvergaard (GT) constitutive model (Xia and Shih, 1995; Ruggieri and Dodds, 1996) given by

$$\Phi = \left(\frac{\sigma_e}{\bar{\sigma}}\right)^2 + 2q_1 f \cosh\left(\frac{3q_2\sigma_m}{2\bar{\sigma}}\right) - \left(1 + q_1^2 f^2\right) = 0 \qquad (1)$$

where σ_e denotes the effective Mises stress, σ_m is $\frac{1}{3}$ of stress tensor trace (hydrostatic stress), $\bar{\sigma}$ is the current flow stress of the cell material and f defines the current void fraction. Factors q_1 and q_2, introduced by Tvergaard, improve the model predictions for interaction among multiple-voids. For the present study, typical values found in bibliography were considered for, q_1 =1.25, q_2=1.0 and D=0.2mm parameters of the computational cells.

Material outside the computational cell layer follows a conventional J_2 flow theory of plasticity and remains undamaged. The crack extension occurs when the current void fraction f reaches a critical value ($f = f_c = 0.1$) in any computational cell. In this case WARP3D eliminate the remaining nodal forces of the cell using a traction separation model. For additional information about the computational cell methodology, reference is made to the works (Xia and Shih, 1995; Ruggieri and Dodds, 1996).

2.2 Modeling of Circumferentially Cracked Pipes

The 3D pipe models have relative crack depth to thickness, a/t = 0.225 and a crack depth to crack length ratio, a/c = 0.3 (axc = 4.5x15mm). The outside diameter and wall thickness of the studied pipes are 323.9 mm and 14.3 mm respectively. Figure 2 shows one of the finite elements models constructed for the 3D analysis of flawed pipes. Reflective symmetry about the crack plane and the mid plane enables the construction of one-quarter model as indicated in the figure. The flaw has a semi-elliptical shape. The 3D pipe models have around 22,000 first

order hexahedron elements (28,000 nodes).

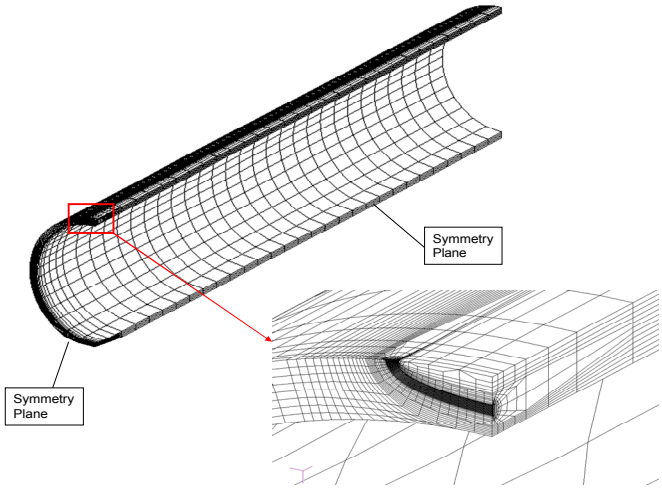

Figure 2: 3D finite element model used in crack growth analyses of the cracked pipe.

In order to study the biaxial effects, the pipes are submitted to increasing curvature and different levels of internal pressure. The maximum curvature imposed to the pipes produces longitudinal strains of around 2% at the outer fiber. The considered internal pressures produce circumferentially (hoop) stresses of 10, 20 and 50% of the material yield stress. The end cap effects were not included in the analyses. The tearing numerical simulation of the pipe was adjusted with experimental data obtained using SENT specimens.

2.3 Modeling of SENT Specimens

FE models of clamped (no rotation at grips) SENT specimens were constructed. The width of the analyzed specimens is W = 13mm, the ratio of specimen thickness over specimen width is, B/W = 2, the relative specimen length is, H/W = 10 and the relative crack size is, a/W = 0.225. Figure 3 shows the FE model constructed for the SENT geometry. Reflective symmetry about the crack plane (y = 0) and the mid plane (z = 0) enables the use of one-quarter models as indicated in the figure. The mesh consists of 8−node, hexahedron isoparametric elements arranged in 15 variable thickness layers. The thinner layers define the near free surface to accommodate the strong variation of the stress and strain fields in the z direction. The 3D SENT models have around 18,000 elements (20,000 nodes).

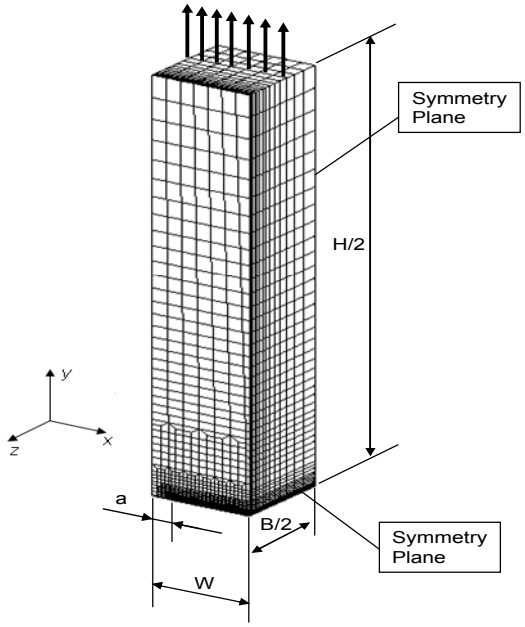

Figure. 3: 3D finite element model of the SENT specimen for crack growth analysis.

2.4 Adjustment of the Model

Fracture toughness results obtained in SENT samples of the *OD* 323.9 x *wt* 14.3 mm pipe were considered. Figure 4 presents the fracture toughness results in terms of J vs. crack growth, Δa. Experimental Δa was obtained as an average value according to the procedure established in ASTM 1820 (ASTM, 2008).

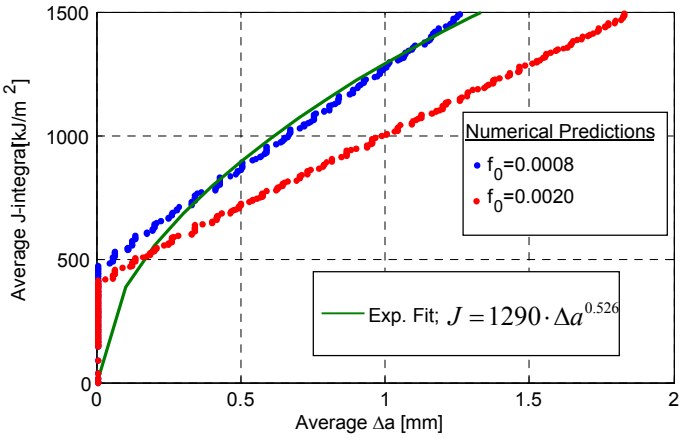

Figure 4: Comparison of experimental resistance curve with the numerical predictions.

The experimental data points were best fitted using a power law given by the ASTM 1820 standard.

The previously presented model of ductile tearing was applied for this case. The experimental results were used to adjust the parameter f_0 (initial relative porosity) of the model. The best fit was found for an initial relative porosity of 0.0008.

The amount of crack growth of the SENT numerical model was obtained by averaging the crack extension of the individual cell layers that form the crack front. The Δa for each layer

was computed considering the not deformed mesh.

2.5 Model Results

Once the parameter f_0 was adjusted for the SENT geometry using the fracture experimental data, it is possible to use the ductile tearing model to predict the fracture toughness for a pipe subjected to different loading conditions, i.e. different biaxiality levels.

The resistance to crack growth curves is calculated at different positions over the crack front (Figure 5) and loading conditions.

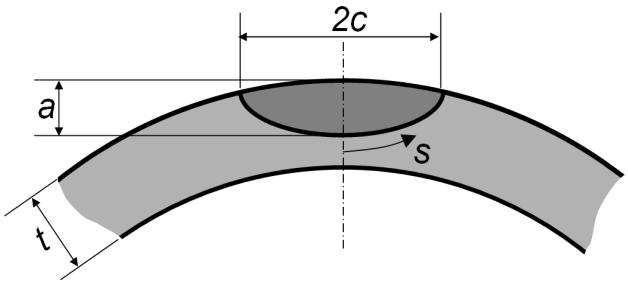

Figure 5: Scheme of circumferential defect and definition of position over the crack front.

Figure 6 presents resistance to crack growth curves as a function of positions over the crack front for the pipe with a/t = 0.225 (axc = 4.5x15mm) subjected to bending without internal pressure. As it can be seen, the resistance curve is insensitive to the position over the crack front. The amount of crack growth in the numerical model of the pipe was measured normal to the crack front.

As can be seen, by comparing Figures 4 and 6, the crack growth results of Figure 4 do not present an initial blunting and Figure 6 does. This is because, in Figure 4 an average Δa is plotted and in Figure 6 a "local" Δa is presented. For the average Δa in Figure 4, the blunting is not apparent because a small growth in the local computations cell layer does not significantly change the average crack growth and, only when an important portion of the crack front starts to growth, the average Δa does it in a significant amount. On the other hand, the "local crack growth" presented in Figure 6 for the pipe, shows an apparent blunting effect because the elimination of a single cell produces a locally significant crack growth.

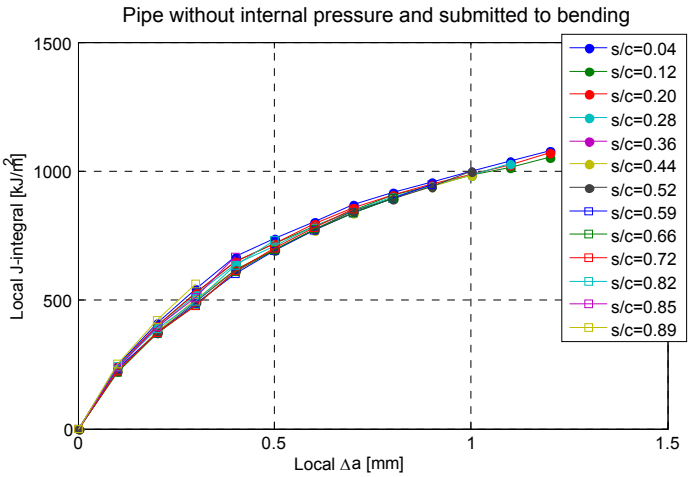

Figure 6: Comparison of resistance curves for different positions over the crack front; Pipe without internal pressure.

Figure 7 presents the resistance curves at the middle of the crack front for the pipe subjected to bending and different levels of internal pressure. The resistance curves are not affected by the biaxiality.

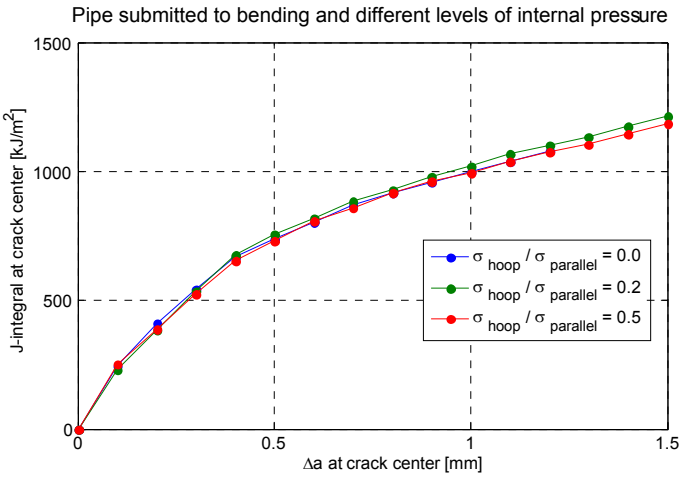

Figure 7: Comparison of resistance curves at the center of the crack for the pipe with different levels of internal pressure.

Crack growth was plotted against the longitudinal deformation of the pipe, as it is shown in Figure 8, for different biaxial loading conditions. As can be seen, for the same longitudinal strain, a higher level of internal pressure causes a larger amount of crack growth.

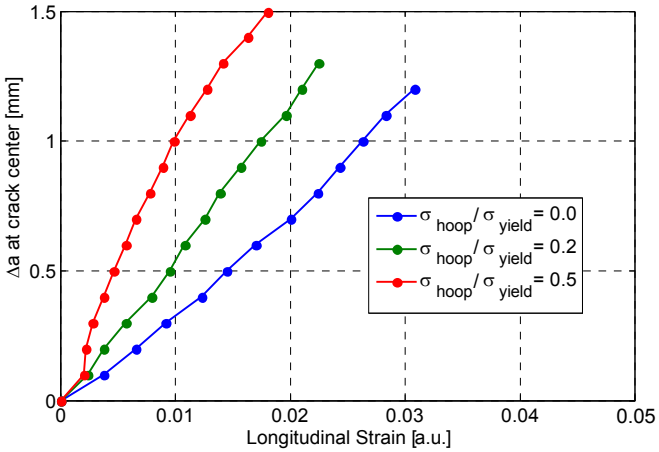

Figure 8: Comparison of crack growth as a function axial strain at the center of the crack for the pipe with different levels of internal pressure.

3 CONSTRAINT EVALUATION

Theoretically, once the parameters of the Gurson-Tvergaard constitutive model are adjusted with an arbitrary geometry, the model may be used to predict ductile tearing in any other configuration. But, in general, there are numerical problems when the geometries considered for the adjustment of the model and the predictions are very different. For this reason, a constraint study must be performed to guarantee that the adjustment of the model with the SENT specimens was properly conducted. Such constraint study, using the *J-Q* methodology and the *h* parameter, developed in a previous work (Cravero et. al., 2008), was considered for this purpose. This study gives information about the characteristics of the crack-tip stress conditions

3.1 J-Q Methodology

In this widely used methodology to compute the constraint loss, the stress field in a finite body is compared with the field from a reference solution constructed for small-scale yielding (SSY) conditions. Commonly the reference solution is the "Boundary Layer" (BL) model (Rice, 1967; Larsson and Carsson, 1973). An approximate two-parameter description for the elastic-plastic crack-tip fields was proposed (O'Dowd and Shih, 1991) based upon a triaxiality parameter applicable under large scale yielding (LSY) conditions. Studying detailed numerical analyses employing the BL model, it was identified (O'Dowd and Shih, 1991) a family of self-similar fields in the form of

$$\sigma_{ij} = \sigma_0 \hat{f}_{ij}\left(\frac{r}{J/\sigma_0}, \theta, Q\right) \tag{2}$$

where the dimensionless Q parameter, defines the amount by which σ_{ij} in a finite body (FB) differs from the reference small scale yielding (SSY) solution. Focusing the stress fields in the region ahead of the crack for the reference solution an the finite body (FB), O'Dowd and Shih showed that $Q\tilde{\sigma}$ corresponds to a spatial uniform hydrostatic stress, i.e., the difference field

relative to a high triaxiality reference stress state

$$\sigma_{ij}^{FB} = (\sigma_{ij})_{SSY;T=0} + Q\,\delta_{1i}\delta_{1j}\ ;\ \text{at}:\ |\theta| < \frac{\pi}{2},\quad J/\sigma_0 < r < 5\,J/\sigma_0 . \tag{3}$$

Operationally, Q is defined by

$$Q \equiv \frac{\sigma_{\theta\theta}^{FB} - \sigma_{\theta\theta}^{SSY}}{\sigma_0};\quad at:\ \theta = 0,\ \ r = \frac{2J}{\sigma_0} \tag{4}$$

where finite element analyses containing sufficient mesh refinement to resolve the fields at this length scale provide the finite body stresses. Here, it is noticed that Q is evaluated at r = $2J/\sigma_0$ for definiteness. However, Q is virtually independent of distance in the range $J/\tilde{\sigma}$ < r < $5J/\tilde{\sigma}$ in the case of tensile loading conditions.

The construction of a *J-Q* trajectory is done by the evaluation of Eq. (3) at each stage of loading in the finite body.

3.2 *h* Parameter for Constraint Characterization

The *J-Q* methodology is suitable to describe constraint condition in cleavage fracture because it only considers effects of constraint over the stress field developed ahead of the crack tip. However, it does not consider the effects of plastic deformations that are important in ductile fracture. The process of stable crack growth in metals can be divided in: 1) nucleation of micro voids, 2) subsequent growth of the same voids, and 3) final coalescence of the micro voids (Garrison and Moody, 1987). Additionally, experimental observations and numerical simulations, demonstrated that plastic deformations associated to the process of void nucleation are small. This allows to simplify the failure process and to assume the growth of cavities as the critical event that controls the ductile tearing in metals.

Based on works of McClintok, 1968 and Rice and Tracey, 1969, that established the growth of micro voids as proportional to $\exp(3\sigma^{\infty}/2\sigma_0)$ where σ^{∞} and $\tilde{\sigma}$ are the remote hydrostatic stress and the yield stress respectively, Brocks and Schmitt (1993) proposed the *h* parameter defined as the ratio of the hydrostatic stress over the effective (Von Mises) stress as a measure of crack tip constrain applicable to ductile fracture,

$$h = \frac{\sigma_h}{\sigma_e}. \tag{5}$$

Here, it is noticed that *h* is evaluated at r = $2J/\tilde{\sigma}$ for definiteness and to be consistent with the evaluation of Q parameter.

3.3 Biaxiality Effects on Constraint Levels of Pipes and Comparison with SENT

The parameters Q and *h* obtained from the middle point of the crack front are representative of the constraint conditions in the studied geometries. The *J-Q* and *J-h* curves of SENT specimens and cracked pipes under different biaxial conditions were compared. Figure 9 shows the evolution of parameter Q with crack-tip loading, *J*, (both values obtained at the center of

the crack front) for the clamped SENT specimen against the cracked pipe with $a/t = a/W = 0.5$.

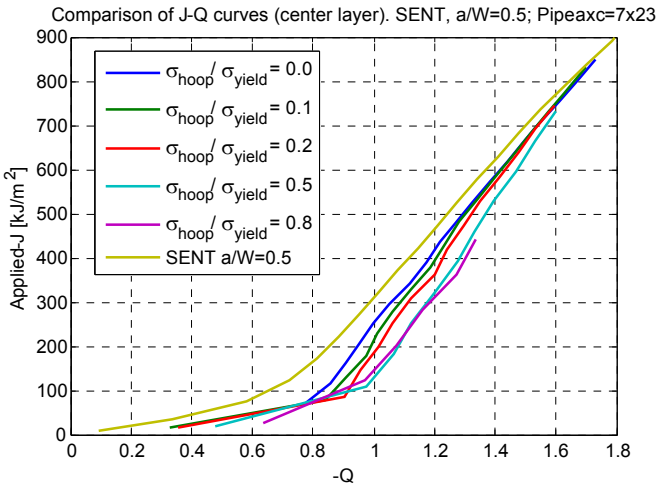

Figure 9: Comparison of J-Q curves between SENT specimen and cracked pipe with different biaxiality levels and a/W = a/t = 0.5.

Figure 10 shows the same results for $a/t = a/W = 0.15$. These analyses show good agreement between the SENT and the pipe level of constraint for the range of crack sizes considered. Furthermore, from Figures 9 and 10, it can be established that the biaxial loading does not significantly modify the level of constraint for the range of loadings and defect sizes considered here.

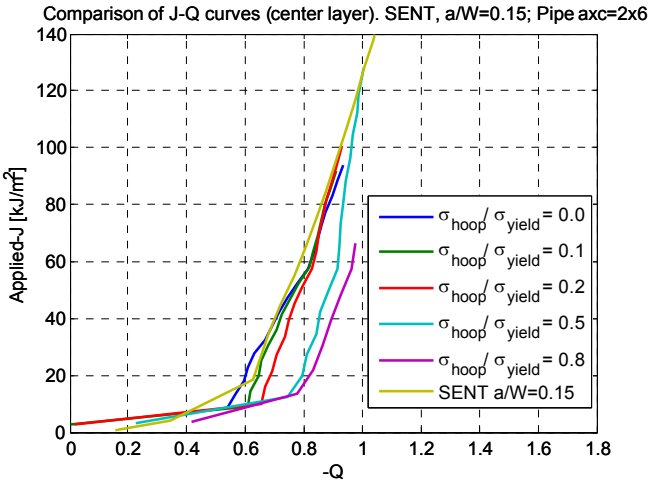

Figure 10: Comparison of J-Q curves between SENT and cracked pipe with different biaxiality levels and a/W=a/t= 0.15.

The same was done for the *J-h* trajectories. Figures 11 and 12 compare the evolution of parameter h with crack-tip loading, J, (both values obtained at the center of the crack front) for the clamped SENT specimen against the cracked pipe. The *J-h* trajectories consider equal relative crack sizes for the SENT specimens and cracked pipes ($a/W = a/t = 0.5$ and 0.15). Again, these analyses show a trend already observed in the previous Figures 9 and 10 with the Q parameter in which the clamped SENT specimen and the cracked pipes exhibit similar levels of crack-tip constraint for the ranges of crack sizes considered. Furthermore, as in the previous

analyses with the *Q* parameter, from Figures 11 and 12, it can be established that the biaxiality level does not significantly modify the level of constraint for the range of loadings considered here. The ranges of *J*-integral represented in the graphs of Figures 9-12, correspond to a curvature of the pipe that causes longitudinal strain from 0 to 2% at the outer fiber.

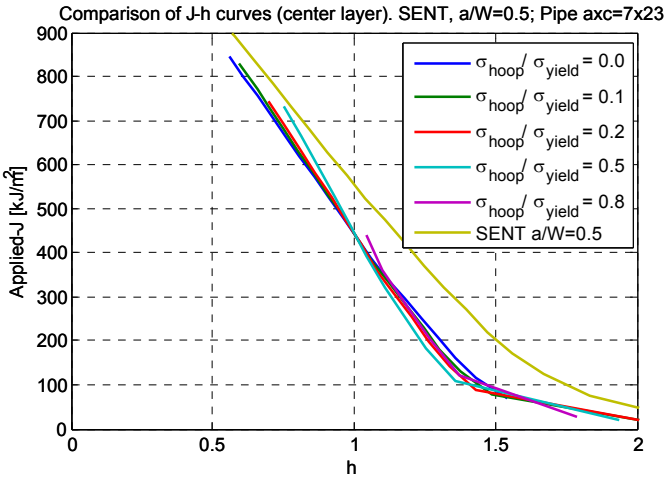

Figure 11: Comparison of J-h curves between SENT specimen and cracked pipe with different biaxiality levels and a/W = a/t = 0.5.

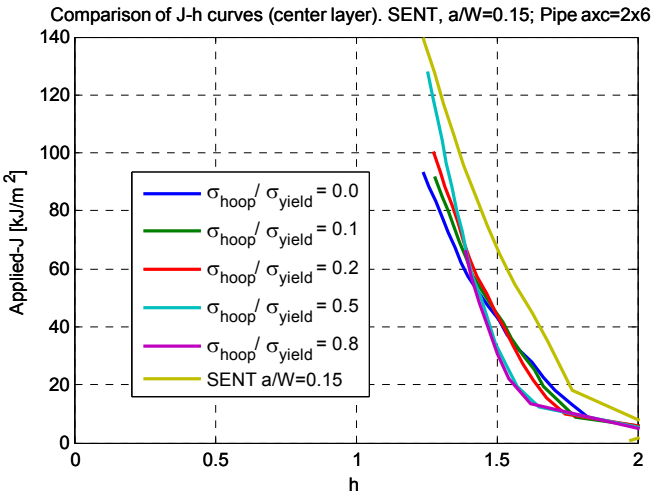

Figure 12: Comparison of J-h curves between SENT specimen and cracked pipe with different biaxiality levels and a/W = a/t = 0.15.

4 DISCUSSION AND CONCLUSIONS

A numerical simulation of ductile tearing in a circumferentially surface cracked pipe under biaxial loading was developed using the computational cell methodology. The model was adjusted with experimental results obtained in laboratory using single edge cracked under tension specimens.

The negligible effect of biaxial loadings on resistance curves was demonstrated. These results indicate that the resistance curve obtained from uniaxial loading can be also applied to biaxial situations. This provides additional support to previous results from Østby and

Hellesvik (2007) and Gioielli et. al. (2007) where full-scale test of pipes submitted to bending and different degrees of internal pressure demonstrated the small effect of biaxiality on resistance curves.

However, for the same longitudinal strain, a higher level of internal pressure causes a larger amount of crack growth, as presented in Figure 8.

The similarities of stress and strains fields between SENT specimens and cracked pipes subjected to biaxial loading were demonstrated by a constraint study using the *J-Q* methodology and the *h* parameter. The levels of constraint ahead of the crack tip are not sensibly modified by the biaxial loading. This fact was verified by the use of the hydrostatic parameter *Q* and the ratio of the hydrostatics stress over the Von Mises stress *h*. The constraint comparison of SENT specimens and pipes indicate the similarity in the fracture condition of these geometries. This result validates the use of SENT specimens in fracture characterization of circumferentially cracked pipes as well when the pipe is submitted to biaxial loading.

5 REFERENCES

ASTM E 1820 – 08: Standard Test Method for Measurement of Fracture Toughness, ASTM, 2008

Brocks W. and Schmitt W., Quantitative Assessment of the Role of Crack Tip Constraint on Ductile Tearing. *Constraint Effects in Fracture, ASTM STP 1171*, American Society for Testing and Materials, pp. 64-78 , 1993.

Cravero S., Bravo R., Ernst H., Evaluation of Crack Tip Constraint in Pipes Subjected to Combined Loading. *Proceedings of the 27th International Conference on Offshore Mechanics and Arctic Engineering*, June 15-20, 2008, Estoril, Portugal.

Garrison, W. M. Jr., Moody, N.R. Ductile Fracture. *Journal of the Physics and Chemistry of Solids*, . 48, pp. 1035−1074, 1987.

Gioielli, P. C, Minnaar, K, Macia, M. L. and Kan, WC, Large-Scale Test Methodology to Measure the Influence of Pressure on Tensile Strain Capacity of a Pipeline. *Proc 17th Int'l Offshore and Polar Eng Conf*, Lisbon, Portugal, 2007.

Koppenhoefer K, Gullerud A, Ruggieri C, Dodds R, Healy B., WARP3D: Dynamic nonlinear analysis of solids using a preconditioned conjugate gradient software architecture. *Structural research series (SRS) 596, UILU-ENG-94-2017*, University of Illinois at Urbana-Champaign, 1994.

Larsson, S. G. and Carlsson, A. J., Influence of Non−Singular Stress Terms and Specimen Geometry on Small Scale Yielding at Crack−Tip in Elastic−Plastic Materials. *Journal of Mechanics and Physics of Solids*, . 21., pp. 263−277, 1973.

McClintok, F. A., A Criterion for Ductile fracture by the Growth of Holes. *Transaction of the ASME, Journal of Applied Mechanics*, . 35, pp. 363-371, 1968.

O'Dowd NP, Shih CF., Family of crack-tip fields characterized by a triaxiality parameter: Part I – structure of fields. *J Mech Phys Solids*, .39, pp.989-1015, 1991.

*Ø*stby E. and Hellesvik A. O., Fracture Control – Offshore Pipelines JIP Results from large scale testing of the effect of biaxial loading on the strain capacity of pipes with defects. *Proceedings of the Seventeenth International Offshore and Polar Engineering Conference ISOPE2007*, Lisbon, Portugal, 2007.

Rice, J. R., Mechanics of Crack Tip Deformation and Extension by Fatigue. *Fatigue Crack Propagation, ASTM STP 415*, American Society for Testing and Materials, pp. 247−309, 1967.

Rice, J. R., A Path Independent Integral and the Approximate Analysis of Strain Concentration by Notches and Cracks. *Journal of Applied Mechanics*, 35, pp. 379−386, 1968.

Rice J. R., Tracey D. M., On the Ductile Enlargement of Voids in Triaxial stress Fields. *Journal of Mechanics and Physics of Solids*, . 17, pp. 201-217, 1969.

Ruggieri, C. and Dodds, R. H., Numerical Modeling of Ductile Crack Growth in 3-D Using Computacional Cell Elements. *International Journal of Fracture*, 82, pp. 67-95, 1996.

Wells, A. A., Unstable Crack Propagation in Metals: Cleavage and fast fracture. *Proceedings of the Crack Propagation Symposium,* 1, Paper 84, Cranfield, UK, 1961.

Xia, L. and Shih, C. F., Ductile Crack Growth − I. A Numerical Study Using Computational Cells with Microstructurally Based Length Scales. *Journal of the Mechanics and Physics of Solids*, 43, pp. 233−259, 1995.